Journal of Alloys and Compounds 509 (2011) 3751–3755

Contents lists available at ScienceDirect

Journal of Alloys and Compounds

journal homepage: www.elsevier.com/locate/jallcom

Temperature-dependent photoluminescence and contactless electroreflectance characterization of a $Zn_xCd_{1-x}Se/Zn_{x'}Cd_{y'}Mg_{1-x'-y'}Se$ asymmetric coupled quantum well structure

J.D. Wu [a], Y.S. Huang [a,*], D.Y. Lin [b], W.O. Charles [c], A. Shen [c], M.C. Tamargo [d], K.K. Tiong [e]

[a] Department of Electronic Engineering, National Taiwan University of Science and Technology, Taipei 106, Taiwan
[b] Department of Electronic Engineering, National Changhua University of Education, Changhua 500, Taiwan
[c] Department of Electrical Engineering, The City College and The Graduate Center of CUNY, New York, NY 10031, USA
[d] Department of Chemistry, The City College and The Graduate Center of CUNY, New York, NY 10031, USA
[e] Department of Electrical Engineering, National Taiwan Ocean University, Keelung 202, Taiwan

ARTICLE INFO

Article history:
Received 13 August 2010
Received in revised form
21 December 2010
Accepted 30 December 2010
Available online 4 January 2011

PACS:
78.30.–j
78.67.De
78.67.pt

Keywords:
Semiconductors
Optical properties
Optical spectroscopy
Contactless electroreflectance
Luminescence

ABSTRACT

Temperature-dependent photoluminescence (PL) and contactless electroreflectance (CER) were used to characterize a $Zn_xCd_{1-x}Se/Zn_{x'}Cd_{y'}Mg_{1-x'-y'}Se$ asymmetric coupled quantum well (ACQW) structure in the range of 10–300 K. The PL peak position yielded information of the fundamental excitonic recombinations. A detailed analysis of the CER spectra led to the identification of various interband transitions. The intersubband transitions were then estimated and found to be in a good agreement with the previous report of Fourier-transform infrared absorption measurements. At low temperature, the PL spectra of the sample showed an asymmetric behavior with an exponential tail at the lower-energy side and were attributed to the localized excitonic recombinations due to potential fluctuations. Detailed study of the temperature dependence of the excitonic transition energies indicated that the main influence of temperature on the quantized transitions is through the temperature dependence of the band gap of the constituent material in the well.

1. Introduction

Quantum cascade lasers (QCLs) that operate in the mid-infrared region are of great interest to the research community because of their potential application in areas such as infrared (IR) imaging and free space telecommunications [1,2]. With this technology, it is possible to produce very narrow linewidth tunable IR sources. As a result, QCLs are ideal for chemical spectroscopy and hence could find applications in areas such as atmospheric pollution monitoring, medicine, and the military. QCLs based on intersubband (ISB) transitions are of great interest due to their potential advantages over those based on interband transition in the IR range. Recently, the observation of electroluminescence emission in quantum cascade (QC) emitter structures made from the II–VI $Zn_xCd_{1-x}Se/Zn_{x'}Cd_{y'}Mg_{1-x'-y'}Se$ grown lattice-matched on InP substrates has been reported [3]. With the absence of intervalley electron scattering, a maximum effective conduction band offset (CBO) of 1.12 eV [4], and the ability of growing high quality $Zn_xCd_{1-x}Se/Zn_{x'}Cd_{y'}Mg_{1-x'-y'}Se$ heterostructures, such as distributed Bragg reflectors [5] and quantum wells (QWs) [6], this material system could be a promising candidate for producing high performance QC emitters operating at a wavelength below 4 μm [3,7].

In this work, we report a detailed study of temperature dependent interband transitions from a $Zn_xCd_{1-x}Se/Zn_{x'}Cd_{y'}Mg_{1-x'-y'}Se$ asymmetric coupled quantum well (ACQW) structure fabricated by molecular beam epitaxy (MBE) using photoluminescence (PL) and contactless electroreflectance (CER) in the range between 10 and 300 K. The PL spectra yield information of fundamental recombination energy. The low temperature PL spectra of the sample showed an asymmetric behavior with an exponential tail at the lower-energy side and were attributed to the localized excitonic recombinations due to potential fluctuations. The derivative nature of CER spectra suppresses uninteresting background effects and

* Corresponding author at: Department of Electronic Engineering, National Taiwan University of Science and Technology, 43 Keelung Road, Section 4, Taipei 106, Taiwan. Tel.: +886 2 27376385; fax: +886 2 27376424.
E-mail address: ysh@mail.ntust.edu.tw (Y.S. Huang).

0925-8388/$ – see front matter © 2011 Elsevier B.V. All rights reserved.
doi:10.1016/j.jallcom.2010.12.207

greatly enhances the precision of interband transition energies. The absence of pump beam in CER avoids certain problems encountered in photoreflectance such as a PL background in high quality samples at low temperature. A number of *mn*H(L) interband transition features are observed in the CER spectra, where *mn*H(L) denotes a transition from the *m*th conduction to *n*th valence subband with heavy (H)- or light (L)-hole character. The study shows that the intersubband transition energies can be estimated by using CER measurements. In addition, the parameters that describe the temperature variation of the excitonic transition energies were evaluated and discussed.

2. Experimental

The multiple ACQW structure was grown by MBE on (0 0 1) semi-insulating InP in a dual chamber Riber 2300P system. The detail growth condition has been described in the previous report [8]. One period of the ACQW structure starting from the spacer layer is made up of the following layers in angstroms: **110**/34/**6**/30. The barrier and spacer layers are shown in boldface. The ACQW were repeated 30 times and the wells were doped with chlorine ($n \sim 4 \times 10^{18}$ cm^{-3}). Doping is needed in order to observe the intersubband absorption by FTIR [8]. The multiple ACQW structure was terminated with the growth of a 291 Å ZnCdSe cap layer. In order to ascertain the growth conditions that would provide the desired doping levels and composition of the well and barrier layers, several calibration samples were grown. The carrier concentration of the doped thick-layer calibration samples was assessed using Hall measurements. The compositions of the well and barrier (or spacer) were determined to be $Zn_{0.48}Cd_{0.52}Se$ and $Zn_{0.24}Cd_{0.18}Mg_{0.58}Se$, respectively, by X-ray diffraction (XRD) measurements at room temperature [8]. The material quality of the ACQW structure was analyzed using high resolution XRD and transmission electron microscopy. The results revealed the excellent structural quality and good control of the well/barrier thickness [8].

PL spectra were excited using the 325 nm line (~50 mW) of a He–Cd laser. The luminescence signals were analyzed by using a Jobin-Yvon "TRIAX 550" spectrometer equipped with a "SIMPHONY" charge coupled device (CCD) camera. In CER experiment an ac modulating voltage (~1 kV at 200 Hz) was applied between a front wire grid electrode and a second electrode consisting of a metal plate. These two electrodes were separated by an insulating spacer in such a manner that there was a very thin layer (~0.1 mm) of air (or vacuum) between the front surface of the sample and the front electrode. Thus, there is nothing in direct contact with the front surface of the sample. The probe beam enters through the front wire grid. The radiation from a 150 W xenon arc lamp filtered by a 0.25 m monochromator provided the monochromatic probe beam. The reflected light was detected by an UV-enhanced silicon photodiode. The dc output of this photodiode was maintained constant by a servomechanism of a variable neutral density filter. A dual-phase lock-in amplifier was used to measure the detected signals. The entire data acquisition procedure has been performed under computer control. Multiple scans over a given photon energy range was programmed until a desired signal-to-noise level has been obtained. For temperature dependent measurements, a closed-cycle cryogenic refrigerator equipped with a digital thermometer controller was used for the low temperature measurements with a temperature stability of 0.5 K or better.

3. Results and discussion

Fig. 1 shows the PL spectra for the ACQW sample in the temperature range between 10 and 300 K. The PL peak monotonically shifts toward lower energy and broadens with increasing temperature in the temperature range from 10 to 300 K. As can be seen in Fig. 1(a), the low temperature PL spectra of the sample show an asymmetric lineshape with an exponential tail at the lower-energy side, a characteristic of localized excitonic recombinations due to potential fluctuations [9]. Several studies have shown that random fluctuations of the alloy composition and roughness of the barrier-well interfaces are the deterministic factors of sample quality for QW heterostructures [9–12]. These defects create fluctuations in the confinement potential and lead to the formation of a band tail in the excitonic density of states [9]. Depending on the energy excess (the laser source) and the magnitude of the potential fluctuation, the excitons will relax either to the local minima or to the absolute minimum of the confinement potential via phonon emission before radiative recombination can take place [13]. The lineshape of PL spectra at lower temperatures causes some difficulties for determining the excitonic recombination energies accurately. We

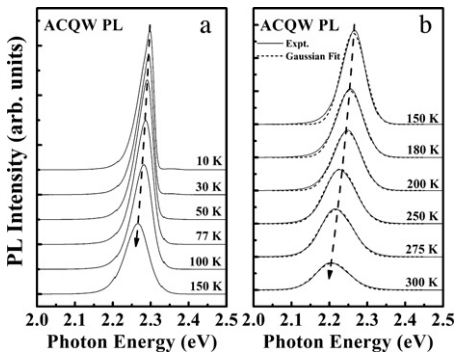

Fig. 1. The PL spectra for the $Zn_{0.48}Cd_{0.52}Se/Zn_{0.24}Cd_{0.18}Mg_{0.58}Se$ sample in the temperature range between 10 and 300 K. (a) The PL spectra at 10, 30, 50, 77, 100, and 150 K. The spectra at low temperatures show an asymmetric lineshape with an exponential tail at the lower-energy side. (b) The PL spectra between 150 and 300 K. The lineshape of the PL spectra at $T \geq 150$ becomes a characteristic lineshape of the recombination of the free excitons which can be fit well by Gaussian lineshape (dashed lines).

therefore assume the peak position to be the energy of 11H recombination.

As shown in Fig. 1(b), for temperature higher than 150 K, the thermal energy prevents the exciton localization, and the lineshape of the PL spectrum becomes a characteristic lineshape of the recombination of the free excitons which can be well fitted by a Gaussian lineshape.

In Fig. 2(a) and (b), the dashed curves represent the experimental CER spectra at 300 and 10 K, respectively. For comparison purpose, the PL spectra at 300 and 10 K are also included in Fig. 2(a) and (b), respectively. The solid curves are the least-squares fits to a derivative Lorentzian lineshape function form [14,15]:

$$\frac{\Delta R}{R} = \mathrm{Re}\sum_{j=1} A_j e^{i\Phi_j}(E - E_j + i\Gamma_j)^{-n}, \quad (1)$$

where A_j and Φ_j are the amplitude and phase of the lineshape, E_j and Γ_j are the energy and broadening parameters of the transitions and the value of n depends on the origin of signatures for the direct band-to-band transition and spin-orbit splitting to band transition of ZnCdSe, denoted as E_0(ZnCdSe) and $E_0 + \Delta_0$(ZnCdSe), are more consistent with $n = 2.5$, while the features originating from ACQWs interband transitions have better fit with $n = 2$. The obtained inter-

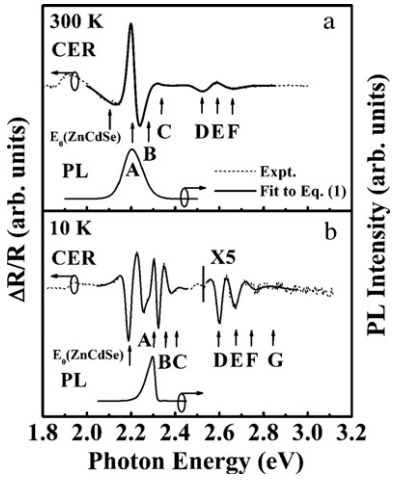

Fig. 2. The experimental CER spectra (short dashed curves) at 300 and 10 K of the $Zn_{0.48}Cd_{0.52}Se/Zn_{0.24}Cd_{0.18}Mg_{0.58}Se$ ACQW structure. The solid curves are the least squares fits to Eq. (1). The 300 and 10 K PL spectra, used to identify the 11H interband transition, are also included.

Table 1
Experimental and theoretical values of the various interband transition energies of the $Zn_{0.48}Cd_{0.52}Se/Zn_{0.24}Cd_{0.18}Mg_{0.58}Se$ ACQW structure at 300 and 10 K. The structure and the conduction band offset are assumed to be **110**/37.4/**6.6**/33 Å and 0.80, respectively, for calculation.

Spectral feature	Transition	300 K				10 K			
		Experiment		Theory		Experiment		Theory	
		E (eV)±0.005	E–E_{11H} (meV)±10	E (eV)	E–E_{11H} (meV)	E (eV)±0.004	E–E_{11H} (meV)±8	E (eV)	E–E_{11H} (meV)
A	11H[a]	2.206	0	2.200	0	2.306	0	2.303	0
	11H[b]	2.205				2.298			
B	22H[a]	2.257	52	2.248	48	2.349	43	2.354	51
C	22L[a]	2.315	109	2.306	106	2.407	101	2.412	109
D	$E_0 + \Delta_0$(ZnCdSe)[a]	2.530				2.620			
E	33H[a]	2.577	371	2.571	371	2.669	363	2.674	371
F	42H[a]	2.651	445	2.652	452	2.743	437	2.748	445
G	44H[a]			2.742	542	2.840	534	2.845	542

[a] CER fitted data.
[b] PL peak position.

band energies at 300 and 10 K of the features denoted A–G are indicated by arrows at the bottom of the figures and summarized in Table 1. It is interesting to note that at 10 K the linewidth of the spectra become sufficiently narrow, so that the structures in the spectrum such as B and C, E and F signals, which are not well resolved at 300 K, become distinguishable in the low-temperature spectrum. Thus more information can be obtained from low temperature spectrum than the room temperature spectrum.

Assignment of the transitions was done according to the following considerations. At room temperature, the signal at 2.090 ± 0.005 eV was assigned to the band gap E_0 of the $Zn_{0.48}Cd_{0.52}Se$ (cap). The value of spin–orbit splitting, Δ_0 = 0.44 eV, was adopted from the similar Zn content of ZnCdSe ternary compound [16]. Using our value of band gap E_0 and this value of Δ_0, we obtained $E_0 + \Delta_0$ = 2.530 ± 0.005 eV for $Zn_{0.48}Cd_{0.52}Se$, which shows good agreement with the experimental value of Table 1. The band gap of the barrier 3.03 eV was obtained with the calibration sample. Comparing the PL spectrum at RT, included in Fig. 2(a) and in Table 1, the dominant CER feature at 2.206 eV is assigned as the 11H interband transition.

To assign the remaining transitions, a calculation was performed based on the envelope function approximation, considering that the QW was doped [8,17]. The values for the effective masses and spin-orbit splitting were obtained from a linear interpolation of the binary values listed in Ref. [18]. We have assumed that the CBO is 0.80 [19] of the band gap difference between the barriers and wells. It should be noted that the CBO for the materials compositions used in this experiment was estimated to be 715 meV, less than the maximum CBO possible with this material system. In order to achieve the maximum CBO available from these materials of 1.12 eV, barrier layers with higher Mg content, up to the maximum lattice-matched composition of $Zn_{0.05}Mg_{0.95}Se$, may be used [4]. The calculated transition energies are listed in Table 1 and the values agree well with the measured values by assuming the structure of ACQW to be **110**/37.4/**6.6**/33 Å.

The E4–E1, E3–E1 and E3–E2 intersubband transition energies of the ACQW sample can be estimated to be 437, 301 and 256 meV, respectively. For example, the difference in energy between the 22H and the 33H interband transitions is 320 meV. Assuming that 80% of this energy difference is in the CB, we estimate that the E3–E2 intersubband transition energy would be about 256 meV. A simulation using the NEXTNANO^3 simulation package [20] was performed to determine the energy level distribution of the CB within the ACQW structure. The schematic of the energy levels and distribution of electron wavefunctions of the CB within the ACQW structure are shown in Fig. 3. The calculated E1, E2, E3, and E4 energy level are 0.097, 0.141, 0.371, and 0.486 eV, respectively. By using this information, a comparison was made between the predicated transitions and they are shown in Table 2. For comparison purpose previous report of the FTIR data obtained from the same sample [8] are also listed in Table 2. Reasonable agreements among the CER estimations, FTIR experimental results and theoretical simulation are observed. The results have shown that CER is a powerful nondestructive technique for characterization of the wide band gap II-VI ACQW structures for QC emitter applications and can be used to accurately predicate intersubband transition energies of the ACQW structures.

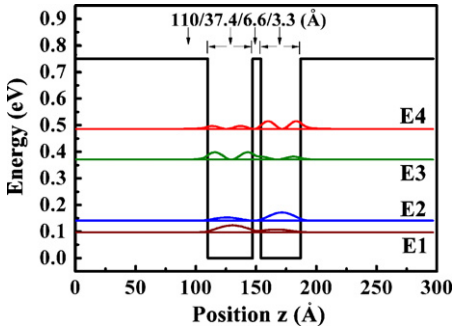

Fig. 3. The schematic of the energy levels and distribution of electron wavefunctions of the ACQW structure simulated by using the NEXTNANO^3 simulation package [20].

Fig. 4 depicts the integrated PL intensity as a function of reciprocal temperature. The integrated PL intensities remain constant between 10 and 50 K. In the higher-temperature regions above 50 K, the exponentially decreasing integrated PL intensities are mainly due to the thermally activated nonradiative recombination channel. The temperature dependence of the integrated intensity of the PL spectra in the QW heterostructures with low defect density is usually described by a phenomenological expression [21]:

$$I_{PL}(T) = \frac{I_0}{1 + A\exp(-E_a/kT)}, \quad (2)$$

Table 2
The intersubband transition energies deduced from CER measurements and theoretical simulation of the $Zn_{0.48}Cd_{0.52}Se/Zn_{0.24}Cd_{0.18}Mg_{0.58}Se$ ACQW structure.

Intersubband transitions	Estimated from CER (meV)[a] ±10 meV	FTIR (meV)[b] ±5 meV	Theoretical simulation (meV)
E2–E1	41		44
E3–E2	256	238	230
E3–E1	297	283	274
E4–E1	435	402	389

The FTIR data are also included for comparison.
[a] Present work.
[b] Ref. [8].

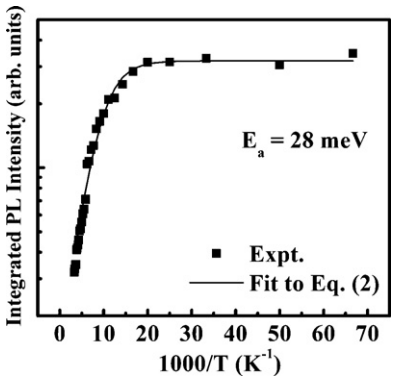

Fig. 4. The integrated PL intensity as a function of reciprocal temperature. The solid line represents the least-squares fit to Eq. (2).

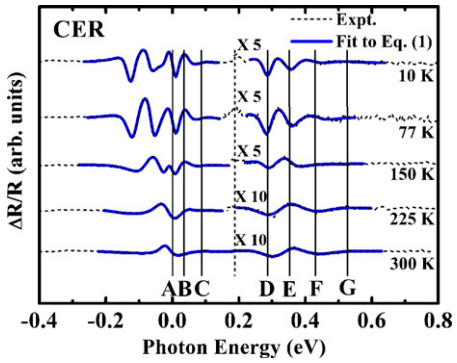

Fig. 6. The temperature dependent CER spectra of the $Zn_{0.48}Cd_{0.52}Se/Zn_{0.24}Cd_{0.18}Mg_{0.58}Se$ ACQW structure at 10, 77, 150, 225 and 300 K. The zero of each scans are taken to lie at the 11H transition energy.

where I_0 is the intensity at $T = 0$ K, A is the ratio between the exciton radiative lifetime in the QW and the exciton escape time from the QW to a nonradiative center [10], and E_a is the thermal activation energy of nonradiative center. The solid line in Fig. 4 represents a least squares fit to Eq. (2). The thermal activation energy obtained from the fit is $E_a = 28 \pm 4$ meV.

Fig. 5 shows the integrated PL intensity as a function of laser excitation power density at 10, 77 and 300 K. The relation between the integrated PL intensity I_{PL} and the excitation density I_{exc} can be described by the expression [22]: $I_{PL}(T) \propto (I_{exc})^{\gamma}$, where γ is a fitting parameter. From the literature [23], an analysis of the appropriate rate equations predicted that $\gamma \sim 1$ corresponds to exciton recombination dominated luminescence. The fitted values of γ equal to 1.11, 1.15 and 1.26 at respectively, 10, 77 and 300 K show that at the measured temperature range the luminescence is dominated by exciton recombination.

Shown in Fig. 6 are the CER spectra of the ACQW for the spectral range of large number of IB transitions at 10, 77, 150, 225 and 300 K, respectively. To facilitate comparison of spectra at different temperatures, we have taken the zero of energy of each scan to lie at the 11H transition energy. The identifications denoted by A–G are indicated by arrows at the bottom of the figure. It is noted that there is no obvious change in the relative position of each transition as the temperature is varied.

The temperature dependence of $E_{mn\mathrm{H(L)}}(T)$ is plotted in Fig. 7. The solid lines are the least-squares fits to the Varshni semiempirical relationship [24]:

$$E(T) = \frac{E(0) - \alpha T^2}{\beta + T}, \tag{3}$$

where $E(0)$ are the energies for mnH(L) transition at 0 K, and α and β are the Varshni coefficients. The constant α is related to the electron (exciton)-average phonon interaction and β is closely related to the Debye temperature [24]. The obtained values of $E(0)$, α and β are listed in Table 3. For comparison, we have also listed in Table 3 the values of $E(0)$, α and β for CdSe [25], ZnSe [26], and $Zn_{0.56}Cd_{0.44}Se$ [26] bulks.

We have also fitted the experimental data to the Bose–Einstein expression [25]:

$$E(T) = E(0) - \frac{2a_B}{[\exp(\Theta_B/T) - 1]}, \tag{4}$$

where $E(0)$ is the transition energy of mnH(L) at 0 K, a_B represents the strength of the electron–phonon interaction and Θ_B corresponds to the average phonon temperature. The obtained values of $E(0)$, a_B and Θ_B are listed in Table 3, along with the corresponding values for the direct gaps of CdSe [25], ZnSe [26] and $Zn_{0.56}Cd_{0.44}Se$ [26] bulks. The a_B and Θ_B in our sample are fairly similar to those of ZnCdSe bulk. For heavy holes and light holes there are slight differences in fitted values of a_B and Θ_B. We interpret this as being the result of different effective masses and their temperature dependence. Since the differences are within the probable errors of measurement, a detailed comparison of these parameters is difficult to perform. Therefore, as in the AlGaAs/GaAs heterostructure system [27], the main influence of temperature on the quantized transitions is attributed to the temperature dependence of the band

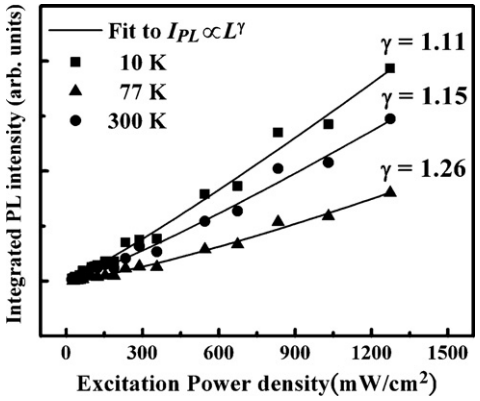

Fig. 5. The integrated PL intensity I_{PL} as a function of laser excitation power density I_{exc} at 10, 77 and 300 K. The solid squares, triangles and circles are the experimental data at 10, 77 and 300 K, respectively. The solid lines are the least-squares fits to the expression of $I_{PL} \propto (I_{exc})^{\gamma}$.

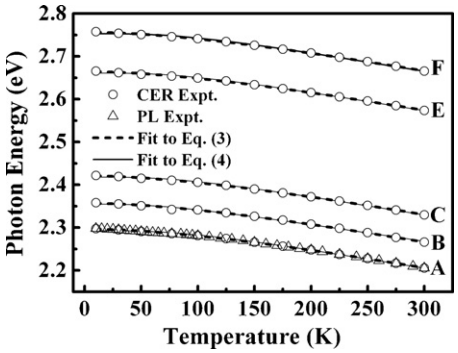

Fig. 7. Temperature dependence of the various interband transition energies for the $Zn_{0.48}Cd_{0.52}Se/Zn_{0.24}Cd_{0.18}Mg_{0.58}Se$ ACQW structure. The dashed lines and solid lines are the least-squares fits to Eqs. (3) and (4), respectively.

Table 3
Values of the parameters which describe the temperature dependence of *mn*H(L) transition energies of $Zn_{0.48}Cd_{0.52}Se/Zn_{0.24}Cd_{0.18}Mg_{0.58}Se$ ACQW structure. The parameters for CdSe, ZnSe and $Zn_{0.56}Cd_{0.44}Se$ are included for comparison.

Materials	*mn*H(L)	$E(0)$ (eV)	α (meV/K)	β (K)	a_B (meV)	Θ_B (K)
$Zn_{0.48}Cd_{0.52}Se/Zn_{0.24}Cd_{0.18}Mg_{0.58}Se$[a]	11H	2.297 ± 0.005	0.55 ± 0.05	245 ± 45	60 ± 4	259 ± 12
	22H	2.357 ± 0.005	0.55 ± 0.05	245 ± 45	60 ± 4	259 ± 12
	22L	2.422 ± 0.005	0.54 ± 0.05	235 ± 50	58 ± 4	252 ± 12
	33H	2.665 ± 0.005	0.55 ± 0.05	245 ± 45	60 ± 4	259 ± 12
	42H	2.757 ± 0.005	0.55 ± 0.05	245 ± 45	60 ± 4	259 ± 12
CdSe[b]	E_0	1.834 ± 0.003	0.42 ± 0.02	118 ± 40	36 ± 5	179 ± 30
ZnSe[c]	E_0	2.800 ± 0.005	0.73 ± 0.04	295 ± 35	73 ± 4	260 ± 30
$Zn_{0.56}Cd_{0.44}Se$[c]	E_0	2.272 ± 0.004	0.61 ± 0.05	206 ± 35	62 ± 4	236 ± 10

[a] Present work.
[b] Ref. [25].
[c] Ref. [26].

gap of the constituent materials in the well. The obtained temperature dependent parameters are important for device applications.

The parameter α of Eq. (3) can be related to a_B and Θ_B in Eq. (4) by taking the high temperature limit of both expressions. The yields $\alpha = 2a_B/\Theta_B$. The comparison of the numbers presented in Table 3 show that this relation is satisfied approximately. From Eq. (4), it is straightforward to show that high temperature limit of the slope of $E(T)$ versus T curve approaches a value of $-2a_B/\Theta_B$. The calculated value of $-2a_B/\Theta_B$ for 11H transition equals to −0.46 meV/K which agrees well with the value of $dE_{11H}/dT = -0.42$ meV/K as obtained from the linear extrapolation of the high temperature (200–300 K) CER and PL experimental data.

4. Summary

In summary, temperature-dependent PL and CER measurements were used to characterize a $Zn_xCd_{1-x}Se/Zn_{x'}Cd_{y'}Mg_{1-x'-y'}Se$ ACQW structure for QC emitter application in the temperature range between 10 and 300 K. The peak position of PL spectrum yields the value of fundamental recombination energy. At low temperature, the PL spectrum of the sample shows an asymmetric behavior with an exponential tail at the lower-energy side and has been attributed to the localized excitonic recombinations due to potential fluctuations. The activation energy of nonradiative channels responsible for thermal quenching is deduced from an Arrhenius plot of the temperature dependent integrated PL intensity. Using CER and theoretical envelope-function approximation calculations, the ground state and higher order interband transitions are observed and identified. Based on the current results, the E4–E1, E3–E1 and E3–E2 intersubband transition energies of the ACQW sample are estimated to be 435, 297 and 256 meV, respectively. Reasonable agreements among the CER estimations, FTIR experimental results and theoretical simulation indicate that CER may be used to accurately predict intersubband transition energies of the ACQW structures. In addition, the parameters that describe the temperature variation of the excitonic transition energies are evaluated. The results indicate that the main influence of temperature on the quantized interband transitions is through the temperature dependence of the band gap of the constituent material in the well. The obtained parameters for the temperature dependence of interband transitions are important for device applications.

Acknowledgments

This work was supported by the National Science Council of Taiwan through Grant No. NSC 98-2221-E-011-015-MY2 and NASA Grant No. NCC-1-03009, NSF Grant No. EEC-0540832 through MIRTHE-ERC, and the Center for Analysis of Structures and Interfaces (CASI).

References

[1] J. Faist, F. Capasso, D.L. Sivco, C. Sirtori, A.L. Hutchinson, A.Y. Cho, Science 264 (1994) 553–556.
[2] M. Beck, D. Hofstetter, T. Aellen, J. Faist, U. Oesterle, M. Ilegems, E. Gini, H. Melchior, Science 295 (2002) 301–305.
[3] K.J. Franz, W.O. Charles, A. Shen, A.J. Hoffman, M.C. Tamargo, C. Gmachl, Appl. Phys. Lett. 92 (2008), 121105 (3 pp.).
[4] M. Sohel, X. Zhou, H. Lu, M.N. Perez-Paz, M.C. Tamargo, M. Muñoz, J. Vac. Sci. Technol. B 23 (2005) 1209–1211.
[5] O. Maksimov, S.P. Guo, L. Zeng, M.C. Tamargo, F.C. Peiris, J.K. Furdyna, J. Appl. Phys. 89 (2001) 2202–2207.
[6] H. Lu, A. Shen, M.C. Tamargo, W. Charles, I. Yokomizo, M. Muñoz, Y. Gong, G.F. Neumark, K.J. Franz, C. Gmachl, C.Y. Song, H.C. Liu, J. Vac. Sci. Technol. B 25 (2007) 1103–1107.
[7] W.O. Charles, K.J. Franz, A. Shen, Q. Zhang, Y. Gong, B. Li, C. Gmachl, M.C. Tamargo, J. Cryst. Growth 310 (2008) 5380–5384.
[8] J.D. Wu, C.T. Huang, Y.S. Huang, W.O. Charles, A. Shen, M.C. Tamargo, Appl. Phys. Lett. 95 (2009), 191905 (3 pp.).
[9] R. Cingolani, F. Sogawa, Y. Arakawa, L. Vanzetti, L. Sorba, A. Franciosi, Appl. Phys. Lett. 73 (1998) 148–150.
[10] S.A. Lourenco, I.F.L. Dias, L.C. Pocas, J.L. Duarte, J.B.B. de Oliverira, J.C. Harmand, J. Appl. Phys. 93 (2003) 4475–4479.
[11] M. Dina, J.E. Cunningham, F. Quochi, J. Shan, J. Appl. Phys. 94 (2003) 1506–1512.
[12] I.A. Buyanova, W.M. Chen, G. Pozina, J.P. Bergman, B. Monemar, H.P. Xin, C.W. Tu, Appl. Phys. Lett. 75 (1999) 501–503.
[13] H.P.D. Schenk, M. Leroux, P. de Mierry, J. Appl. Phys. 88 (2000) 1525–1534.
[14] F.H. Pollak, H. Shen, Mater. Sci. Eng. R 10 (1993), xv–xvi.
[15] D.E. Aspnes, in: T.S. Moss, M. Balkanski (Eds.), Handbook on Semiconductors, vol. 2, North-Holland, Amsterdam, 1980, pp. 109–154.
[16] T. Holden, P. Ram, F.H. Pollak, J.L. Freeouf, B.X. Yang, M.C. Tamargo, Phys. Rev. B 56 (1997) 4037–4046.
[17] G. Bastard, J.A. Brum, IEEE J. Quant. Electron. QE-22 (1986) 1625–1644.
[18] O. Madelung, M. Schultz, H. Weiss (Eds.), Semiconductors, Landolt-Börnstein, New Series, Group III, vol. 17b, Springer, New York, 1982.
[19] H. Lu, A. Shen, W. Charles, I. Yokomizo, M.C. Tamargo, K.J. Franz, C. Gmachl, M. Muñoz, Appl. Phys. Lett. 89 (2006), 241921(3 pp.).
[20] NEXTNANO^3 nextgeneration 3D device simulator, the program is available at: http://www.nextnano.de/nextnano3.
[21] O. Maksimov, S.P. Guo, M. Muñoz, M.C. Tamargo, J. Appl. Phys. 90 (2001) 5135–5138.
[22] M. Yin, G.R. Nash, S.D. Coomber, L. Buckle, P.J. Carrington, A. Krier, A. Andreev, S.J.B. Przeslak, G. de Valicourt, S.J. Smith, M.T. Emeny, T. Ashley, Appl. Phys. Lett. 93 (2008), 121106 (3 pp.).
[23] J.E. Fouquet, A.E. Siegman, Appl. Phys. Lett. 46 (1985) 280–282.
[24] Y.P. Varshni, Physica (Utrecht) 34 (1967) 149–154.
[25] S. Logothetidis, M. Cardona, P. Lautenschlager, M. Garriga, Phys. Rev. B 34 (1986) 2458–2469.
[26] L. Malikova, W. Krystek, F.H. Pollak, N. Dai, N.A. Cavus, M.C. Tamargo, Phys. Rev. B 54 (1996) 1819–1824.
[27] A. Kangarula, H.R. Chandrasekhar, M. Chandrasekhar, Y.M. Kapoor, F.A. Chambers, B.A. Vojak, J.M. Meese, Phys. Rev. B 37 (1988) 1035–1038.